Hardware-Efficient Coherent Digital Receiver Concept With Feedforward Carrier Recovery for M-QAM Constellations

Timo Pfau, *Student Member, IEEE*, Sebastian Hoffmann, and Reinhold Noé, *Member, IEEE*

***Abstract*—This paper presents a novel digital feedforward carrier recovery algorithm for arbitrary M-ary quadrature amplitude modulation (M-QAM) constellations in an intradyne coherent optical receiver. The approach does not contain any feedback loop and is therefore highly tolerant against laser phase noise. This is crucial, especially for higher order QAM constellations, which inherently have a smaller phase noise tolerance due to the lower spacing between adjacent constellation points. In addition to the mathematical description of the proposed carrier recovery algorithm also a possible hardware-efficient implementation in a parallelized system is presented and the performance of the algorithm is evaluated by Monte Carlo simulations for square 4-QAM (QPSK), 16-QAM, 64-QAM, and 256-QAM. For the simulations ASE noise and laser phase noise are considered as well as analog-to-digital converter (ADC) and internal resolution effects. For a 1 dB penalty at $\mathrm{BER} = 10^{-3}$, linewidth times symbol duration products of 4.1×10^{-4} (4-QAM), 1.4×10^{-4} (16-QAM), 4.0×10^{-5} (64-QAM) and 8.0×10^{-6} (256-QAM) are tolerable.**

***Index Terms*—Coherent communication, feedforward carrier recovery, optical communication, parallel processing, phase estimation, phase noise, quadrature amplitude modulation.**

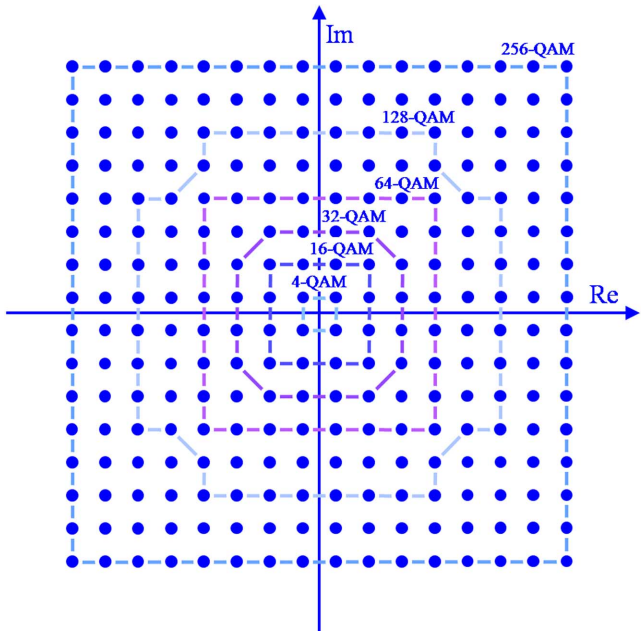

Fig. 1. Square QAM constellation diagrams.

I. Introduction

QUADRATURE amplitude modulation in combination with coherent detection is very attractive for future optical transmission systems, since it allows to increase the data rate without increasing the symbol rate or the required bandwidth. This allows integrating single wavelength channels with data rates at 100 Gb/s and above into existing dense wavelength division multiplexed (DWDM) systems with 50 GHz spacing. Additionally, as the throughput for coherent transmission systems is strongly limited by the ADC bandwidth and sampling rate, higher order QAM modulation formats reduce these requirements.

Tremendous studies have already been done on coherent quadrature phase shift keying (QPSK) [1], [2], which can also be regarded as 4-QAM, and first realtime transmission systems have already been demonstrated [3]–[5]. Also higher order QAM modulation formats (see Fig. 1) attract more and more attention. Integrated modulators have already been developed for 16-QAM [6], [7], and the transmission of a polarization-multiplexed 128-QAM signal was demonstrated using a pilot carrier for optical phase noise cancelling [8].

However, a linewidth tolerant feed-forward carrier recovery avoiding feedback loops for higher-order QAM constellations has not been proposed so far. The published algorithms either contain a decision directed feedback loop [9]–[11], use only dedicated symbols for carrier recovery that fulfill certain criteria [12] or perform differential decoding without carrier recovery [13]. The first two approaches achieve only a low laser linewidth tolerance in practical systems prohibiting the utilization of standard distributed DFB lasers. The latter has a lower receiver sensitivity due to the asynchronous detection.

In this article we present a hardware-efficient and phase noise tolerant feedforward carrier recovery concept for synchronous decoding of arbitrary M-QAM constellations. The feedbackless algorithm is described mathematically and a hardware-efficient implementation is proposed. The performance of the algorithm is investigated for 4-QAM (QPSK), 16-QAM, 64-QAM and 256-QAM in Monte Carlo simulations (Fig. 1). The implementation of 32-QAM and 128-QAM is also possible but not addressed in this article. The simulations consider laser phase noise effects, but also various quantization effects in the

Manuscript received August 01, 2008; revised November 20, 2008, October 23, 2008. Current version published April 17, 2009.

The authors are with the Optical Communication and High-Frequency Engineering, University of Paderborn, 33098 Paderborn, Germany (e-mail: pfau@ont.upb.de; hoffmann@ont.upb.de; noe@upb.de).

Digital Object Identifier 10.1109/JLT.2008.2010511

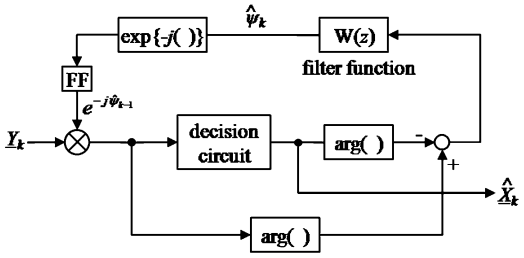

Fig. 2. Decision-directed carrier recovery with $\Delta = 1$.

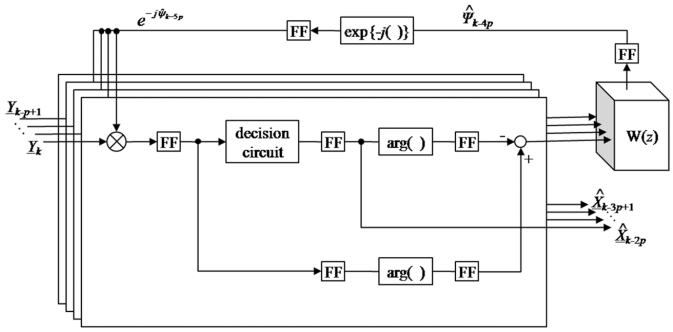

Fig. 3. Decision-directed carrier recovery in a parallelized and pipelined receiver ($\Delta \gg 1$).

receiver. The results show that a practical implementation of 16-QAM using DFB lasers is already possible today, therefore being a potential candidate for 100 Gb/s transmission systems. 64-QAM and 256-QAM can be realized in the near future and may enable 400 Gb/s transmission in 50-GHz-spaced DWDM channels.

II. Phase Noise Tolerance of Decision-Directed Digital Carrier Recovery Concepts for M-QAM Constellations

Phase noise can be modeled as a Wiener process [14]

$$\psi_k = \sum_{i=-\infty}^{k} f_i, \tag{1}$$

where the f_i's are independent and identically distributed random Gaussian variables with zero mean and variance

$$\sigma_f^2 = 2\pi(\Delta f \cdot T_S). \tag{2}$$

Δf is the sum linewidth of signal and local oscillator lasers and T_S is the symbol period.

Fig. 2 shows the general structure of a decision-directed carrier & data recovery module with feedback delay $\Delta = 1$. The phase estimator uses the estimated carrier phase $\hat{\psi}_{k-1}$ to derotate the symbol Z_k, and the result is fed into a decision device ($[]_D$ denotes the output of the decision device).

$$\hat{X}_k = [Z'_k]_D = [Z_k \exp\{-j\hat{\psi}_{k-1}\}]_D, \tag{3}$$

The carrier phase estimate $\hat{\psi}_k$ is calculated with

$$\hat{\psi}_k = \sum_{i=0}^{N} w_i(\arg\{Z_{k-i}\} - \arg\{\hat{X}_{k-i}\}), \quad \sum_{i=0}^{N} w_i = 1. \tag{4}$$

where w_i are weighting coefficients (e.g., Wiener filter coefficients) and N is the FIR filter length. If only preceding symbols are used as inputs to the FIR filter, a feedback delay of $\Delta = 1$ becomes theoretically possible [10].

However, in a practical implementation it is impossible to achieve $\Delta = 1$. A real circuit implementation that supports 100 Gb/s or higher data throughput, will use massive parallelization and pipelining to realize a synchronous carrier and data recovery. Parallelization means that the received samples are demultiplexed into several parallel modules to be able to process the data at a lower clock speed. Pipelining signifies that the whole carrier recovery process is not executed completely within one clock cycle, but only fractions of the processing are performed and the auxiliary results are stored in registers or flip-flops (FF). Fig. 3 shows the structure of such an implementation. It can be seen that due to the parallel processing of p consecutive samples the feedback delay between two symbols within one module is equal to the degree of parallelism p. Even if the latest phase estimate from all parallel outputs is fed back into each module as shown in Fig. 3, the average delay amounts to $(p+1)/2$. Taking also the number of pipeline stages l into account (represented by the flip-flops (FF) in Fig. 3), meaning that it takes l clock cycles until an input sample has an impact on the feedback value, the total average feedback delay is

$$\Delta = (l-1) \cdot p + \frac{p+1}{2}. \tag{5}$$

Note that the minimum number of pipeline stages is 1, because this is the minimum number of clock cycles required in a digital feedback system (cp. Fig. 2).

To determine the effect of Δ on the phase noise tolerance of the receiver, let $\hat{\psi}_{k-\Delta}$ be a perfect estimate of $\psi_{k-\Delta}$, i.e., $\hat{\psi}_{k-\Delta} = \psi_{k-\Delta}$ and Z_k is only corrupted by phase noise. With (3), Z'_k can be written as

$$Z'_k = Z_k \exp\{j(\psi_k - \psi_{k-\Delta})\} = Z_k \exp\{j\psi'_k\}. \tag{6}$$

According to (1) ψ'_k is given by

$$\psi'_k = \psi_k - \psi_{k-\Delta} = \sum_{i=k-\Delta}^{k} f_i. \tag{7}$$

ψ'_k is a random Gaussian variable with zero mean and variance $\sigma_\psi^2 = \Delta \cdot \sigma_f^2 = 2\pi(\Delta \cdot \Delta f \cdot T_S)$. Therefore, the standard deviation of the phase noise increases by the factor $\sqrt{\Delta}$.

In a practical implementation, assuming e.g., parallel processing with $p = 16$ and $l = 5$ pipeline stages, the average feedback delay is $\Delta = 72.5$ samples. This shows that a decision-directed carrier recovery is fairly unfeasible because the phase noise tolerance is reduced by a factor of ~ 8.5. Consequently any feedback loop must be avoided in the carrier recovery process, especially for higher order QAM constellations with their inherently smaller phase noise tolerance. In particular, the carrier cannot be recovered in a decision-directed manner when normal DFB lasers are used.

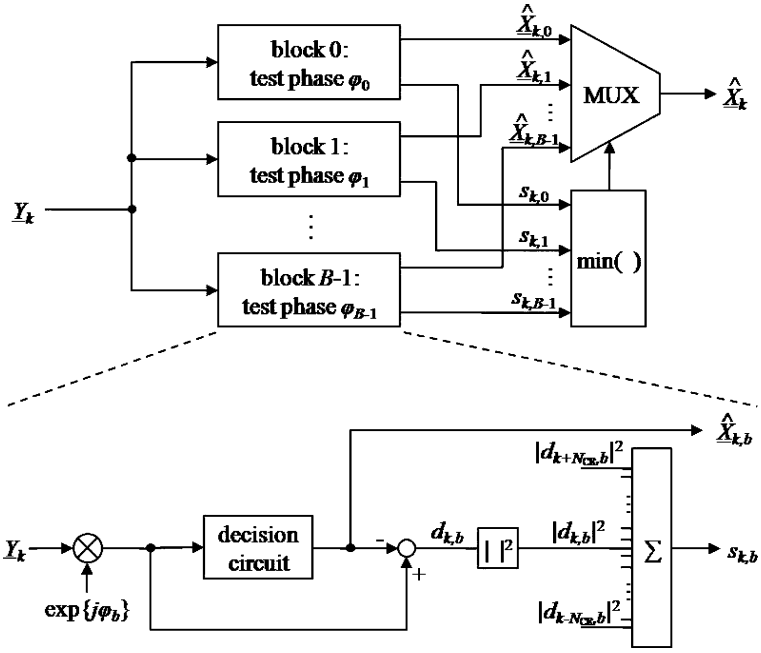

Fig. 4. Feedforward carrier recovery using B test phase values φ_b.

III. Feedforward Carrier Recovery Algorithm

A. Square QAM Constellations

Fig. 4 shows a block diagram of the proposed carrier recovery module. The input signal Z_k of the coherent receiver is sampled at the symbol rate, and perfect clock recovery and equalization are assumed. To recover the carrier phase in a pure feedforward approach the received signal Z_k is rotated by B test carrier phase angles φ_b with

$$\varphi_b = \frac{b}{B} \cdot \frac{\pi}{2}, \quad b \in \{0, 1, \ldots, B-1\}. \tag{8}$$

Then all rotated symbols are fed into a decision circuit and the squared distance $|d_{k,b}|^2$ to the closest constellation point is calculated in the complex plane

$$\begin{aligned} |d_{k,b}|^2 &= |Z_k \exp\{j\varphi_b\} - \lfloor Z_k \exp\{j\varphi_b\} \rfloor_D|^2 \\ &= |Z_k \exp\{j\varphi_b\} - \hat{X}_{k,b}|^2. \end{aligned} \tag{9}$$

In order to remove noise distortions, the distances of $2N+1$ consecutive test symbols rotated by the same carrier phase angle φ_b are summed up

$$s_{k,b} = \sum_{n=-N}^{N} |d_{k-n,b}|^2. \tag{10}$$

The optimum value of the filter half width N depends on the laser linewidth times symbol rate product. $N = 6, \ldots, 10$ will be a fairly good choice.

After filtering the optimum phase angle is determined by searching the minimum sum of distance values. As the decoding was already executed in (9), the decoded output symbol $\hat{X}_k$ can be selected from the $\hat{X}_{k,b}$ by a switch controlled by the index $m_{k,\min}$ of the minimum distance sum.

Due to the 4-fold ambiguity of the recovered phase in the square M-QAM constellation the receiver cannot uniquely assign the $\log_2\{M\}$ bits to the recovered symbol. This problem can be resolved either by using framing information [15] or by applying differential coding [16]. It is sufficient to differentially Gray-encode the two bits that determine the quadrant of the complex plane. The differential encoding and decoding process is the same as for QPSK and is presented in detail in [17]. It can be described by the following formula

$$\begin{aligned} n_{o,k} &= (n_{r,k} - n_{r,k-1} + n_{j,k}) \bmod 4 \\ & \qquad n_{o,k}, n_{r,k}, n_{j,k} \in \{0, 1, 2, 3\} \end{aligned} \tag{11}$$

where $n_{o,k}$ is the differentially decoded quadrant number, $n_{r,k}$ is the received quadrant number and $n_{j,k}$ is the jump number. The only required modification of the decoding process compared to [17] is that quadrant jumps are detected according to the following formula:

$$n_{j,k} = \begin{cases} 1, & \text{if } m_{k,\min} - m_{k-1,\min} > B/2 \\ 3, & \text{if } m_{k,\min} - m_{k-1,\min} < -B/2 \\ 0, & \text{otherwise.} \end{cases} \tag{12}$$

All other bits that determine the symbol within the quadrant of the complex plane are Gray-encoded without any differential encoding or decoding. Fig. 5 exemplifies the bit to symbol assignment including differential encoding/decoding for square 16-QAM.

The resulting constellation diagram is not any more Gray-encoded. This results in a coding penalty, which is 3 dB for 4-QAM (QPSK) and drops to nearly 0 dB for high order constellations [18].

B. Arbitrary QAM Constellations

The proposed feedforward carrier recovery concept can also be applied to arbitrary QAM constellations. If the constellation

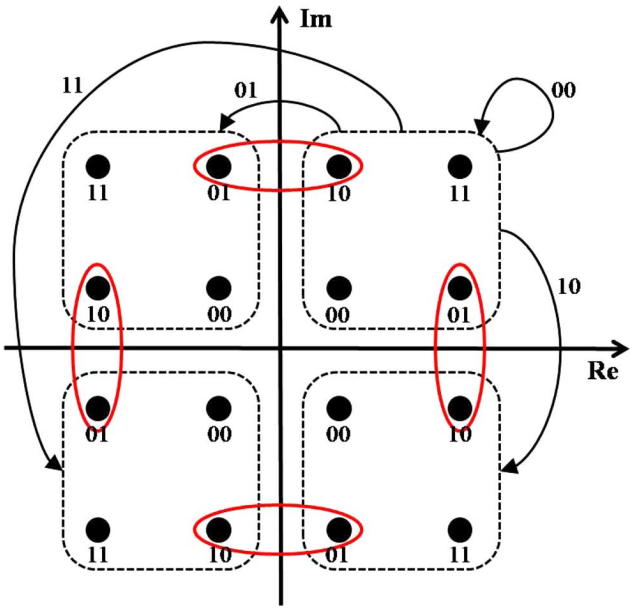

Fig. 5. 16-QAM bit to symbol assignment: The encircled symbol pairs have a Hamming distance larger than 1 due to differential encoding of the quadrant.

diagram is rotationally symmetric by the angle γ, then φ_b must be selected as

$$\varphi_b = \frac{b}{B} \cdot \gamma, \quad b \in \{0, 1, \ldots, B-1\}. \tag{13}$$

For square QAM constellations $\gamma = \pi/2$ [cp. (8)] holds. Without rotational symmetry $\gamma = 2\pi$ must be used.

Due to the k-fold ambiguity of the recovered phase with $k = 2\pi/\gamma$, $\lceil \log_2\{k\} \rceil$ bits should be differentially encoded/decoded, where $\lceil u \rceil$ is the smallest integer larger than or equal to u. (11) therefore changes to the more general expression

$$n_{o,k} = (n_{r,k} - n_{r,k-1} + n_{j,k}) \bmod k$$
$$n_{o,k}, n_{r,k}, n_{j,k} \in \{0, \ldots, k-1\}. \tag{14}$$

C. Polarization Division Multiplexing & Equalization

If polarization division multiplexing is applied, there are two possibilities to implement the carrier recovery. One option is to use two separate carrier recoveries for each polarization, or to have a common carrier recovery for both polarizations as proposed in [19]. To realize this option (10) must be modified as follows:

$$s_{k,b} = \sum_{p=1}^{2} \sum_{n=-N}^{N} |d_{p,k-n,b}|^2 \tag{15}$$

where p is the index of the polarization. Because twice as much data is available to determine the carrier phase angle, N can be halved, increasing the phase noise tolerance roughly by a factor of 2 [19].

The presented feedforward carrier recovery algorithm is compatible with all kinds of equalizers proposed for polarization control, chromatic dispersion (CD) and polarization mode dispersion (PMD) compensation. Both non-decision-aided feedforward equalizers based e.g., on the constant modulus algorithm (CMA) [20] or decision-directed equalization as proposed in [19] can be applied.

IV. Hardware-Efficient Carrier Recovery Implementation

A. Efficient Calculation of Vector Rotations

The rotation of a symbol in the complex plane normally requires a complex multiplication, consisting of four real-valued multiplications with subsequent summation. This would lead to a large number of multiplications to be executed, while achieving a sufficient resolution B for the carrier phase values φ_b. The hardware effort would therefore become prohibitive. Applying the CORDIC (coordinate rotation digital computer) algorithm [21], [22] can dramatically reduce the necessary hardware effort to calculate the B rotated test symbols. This algorithm can compute vector rotations simply by summation and shift operations. As for the calculation of the B rotated copies of the input vector intermediate results can be reused for different rotation angles, only $\sum_{b=1}^{\log_2\{B\}} 2^{b+1}$ shift and add operations are required to generate the B test symbols. For example to generate $B = 32$ rotated copies of Z_k the CORDIC algorithm requires only 124 shift and add operations instead of 124 real valued multiplications and 62 summations.

B. Calculation of the Distance to the Closest Constellation Point

To determine the closest constellation point $\hat{X}_{k,b}$ the rotated symbols are fed into a decision circuit. The square distance $|d_{k,b}|^2$ [(9)] can be written as

$$\begin{aligned} |d_{k,b}|^2 &= (\mathrm{Re}[d_{k,b}])^2 + (\mathrm{Im}[d_{k,b}])^2 \\ &= (\mathrm{Re}[Z_k \exp\{j\varphi_b\}] - \mathrm{Re}[\hat{X}_{k,b}])^2 \\ &\quad + (\mathrm{Im}[Z_k \exp\{j\varphi_b\}] - \mathrm{Im}[\hat{X}_{k,b}])^2. \end{aligned} \tag{16}$$

Implementing this formula literally into hardware would lead to two multipliers and three adders/subtractors. But a closer examination of (9) and (16) reveals that the results of the subtractions are relatively small because the distance to the closest constellation point is calculated. Therefore, the most significant bits (MSBs) of the subtraction result will always be zero and can be discarded to reduce the hardware effort. Due to the moderate required resolution for d^2, the squared distance (15) can be determined by a look-up table or basic logic functions more efficiently than with multipliers.

C. Filter Function

Highly parallelized systems allow a very resourceful implementation of the summation of $2N+1$ consecutive values. The adders can be arranged in a binary tree structure where intermediate results from different modules are reused in neighboring modules leading to a moderate hardware effort.

D. Overall Hardware Effort

To estimate the overall hardware effort, we compare the proposed algorithm against the QPSK carrier recovery algorithm proposed in [17]. Both algorithms contain almost the same functional blocks such as the rotation in the complex plain, the filter function or the decision circuit. Both algorithms also use look-up tables, [17] for calculating the argument of a complex sample, and the newly proposed algorithm to calculate $|d_{k,b}|^2$. The only functional block not found in [17] is the search for the minimum sum of the filter outputs and the subsequent switch. Considering that the complex rotation is more hardware-efficient in the proposed algorithm than in [17], because the CORDIC algorithm can reuse intermediate results, the hardware effort for the proposed algorithm is roughly B times higher than the one for QPSK carrier recovery. It may be viewed as a large increase since B is in the range of 16 to 64. But taking into account that the algorithm is designed for high-order QAM constellations, and that the hardware effort for chromatic dispersion (CD) compensation, polarization mode dispersion (PMD) compensation or polarization control is also many times higher than the hardware effort for [17], the implementation of the proposed algorithm can be achieved with reasonable effort.

V. Square QAM Simulation Results

To evaluate the performance of the proposed carrier recovery algorithm and to determine the required hardware effort, extensive simulations have been carried out. The considered constellations are 4-QAM (QPSK), 16-QAM, 64-QAM and 256-QAM with differential encoding/decoding as described in Section III.A. Our simulations are limited to square constellations because they are more straightforward to generate [6], [7] and optimal in respect of noise immunity in additive white Gaussian noise (AWGN) dominated transmission systems [18]. The filter width is always set to $N = 9$, and each data point is based on the simulation of 200 000 symbols. The results are compared against the theoretically achievable sensitivity with ideal Gray coding. Thus, the sensitivity penalties observed in the simulations take also the coding penalty due to differential encoding/decoding into account. The theoretically achievable sensitivity is calculated with the following formula [18]:

$$\frac{E_S}{N_0} = \frac{M-1}{3}\left(\mathrm{Q}^{-1}\left[\frac{\log_2\{M\}}{2}\left(1-\frac{1}{\sqrt{M}}\right)^{-1} \times \left(1-\sqrt{1-\mathrm{BER}}\right)\right]\right)^2 \quad (17)$$

where E_S is the average energy per symbol, N_0 is the noise power spectral density, M is the number of constellation points and BER is the target bit error rate. E_S/N_0 is referred to as optical signal to noise ratio (OSNR),

A. Phase Angle Resolution

A crucial quantity for the proposed algorithm is the required number B of the test phase values φ_b. If the required resolution is too large, the realization in hardware becomes unfeasible. Fig. 6(a) shows the sensitivity penalty at the bit error rate 10^{-3} for 4-QAM and 16-QAM. The proposed algorithm and a receiver with ideal carrier recovery were simulated with different resolutions for the carrier phase. Ideal carrier recovery means that the receiver knows the exact carrier phase (which is only realizable in simulation) and therefore the sensitivity penalty is

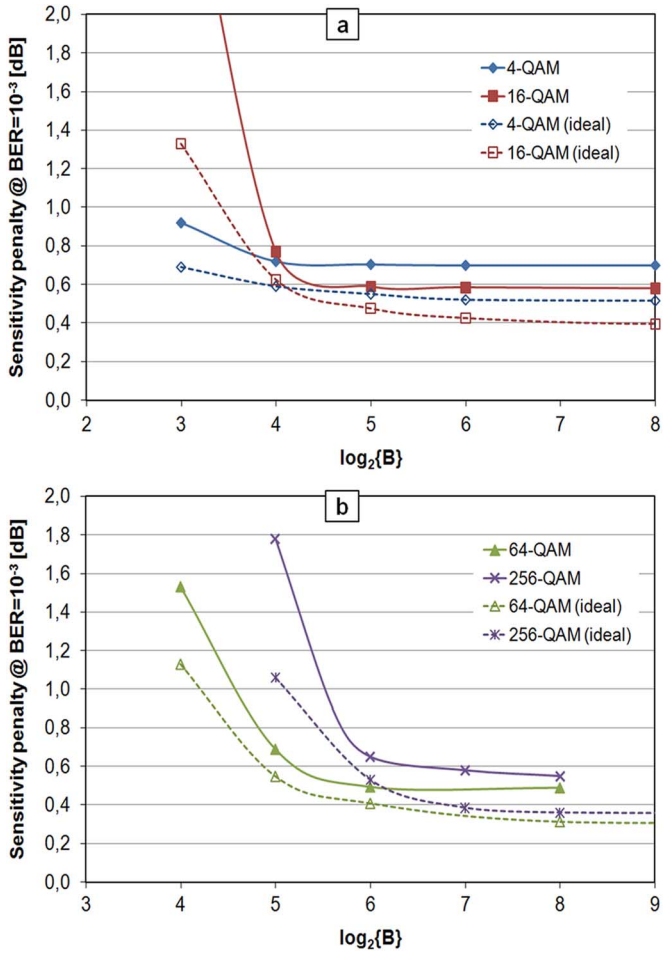

Fig. 6. Sensitivity penalty for different numbers of test phase values φ_b (a) for 4-QAM and 16-QAM; (b) for 64-QAM and 256-QAM.

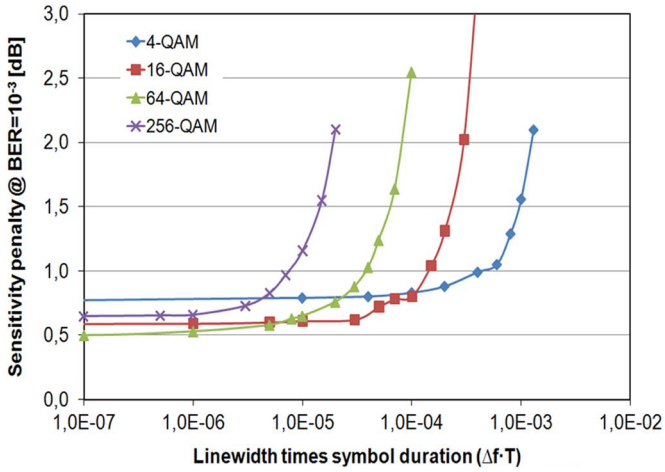

Fig. 7. Receiver tolerance against phase noise for different square QAM constellations.

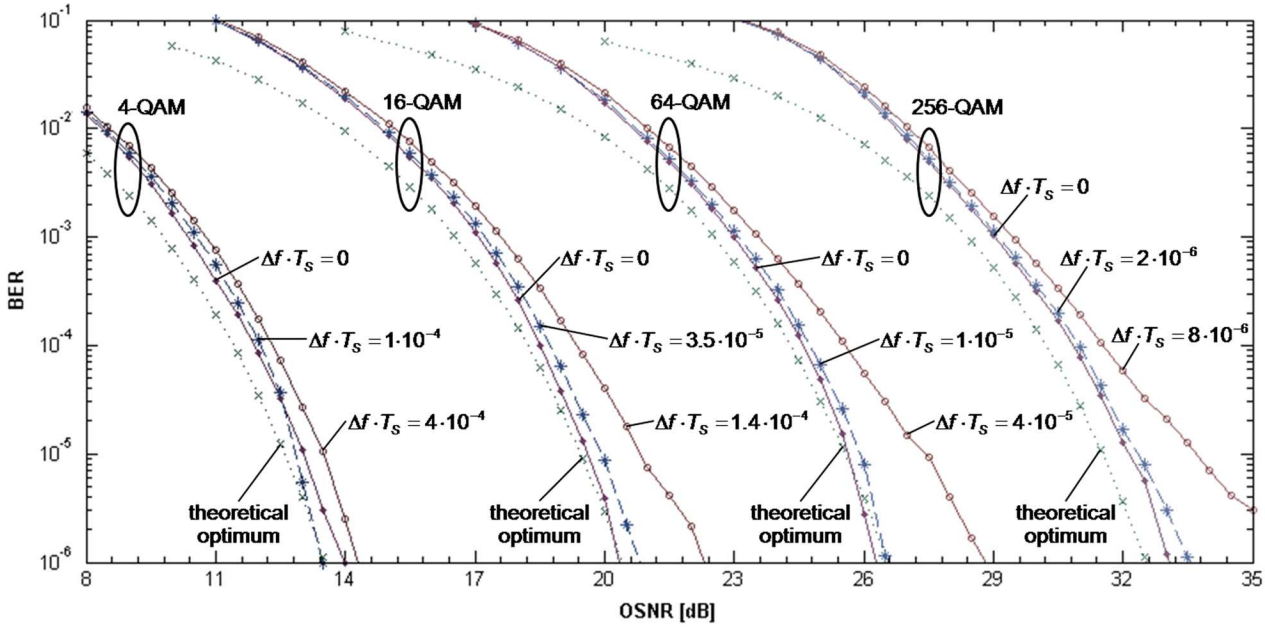

Fig. 8. Impact of different linewidth times symbol duration products on the receiver sensitivity of coherent QAM receivers.

TABLE I
LINEWIDTH REQUIREMENTS FOR FEEDFORWARD CARRIER RECOVERY WITH DIFFERENT SQUARE QAM CONSTELLATIONS

Constellation	Max. tolerable $\Delta f \cdot T_S$ for 1 dB penalty @ BER = 10^{-3}	Max. tolerable Δf for T_S = 10 Gbaud
4-QAM	$4.1 \cdot 10^{-4}$	4.1 MHz
16-QAM	$1.4 \cdot 10^{-4}$	1.4 MHz
64-QAM	$4.0 \cdot 10^{-5}$	400 kHz
256-QAM	$8.0 \cdot 10^{-6}$	80 kHz

only caused by differential quadrant encoding and quantization effects.

4-QAM attains a minimum penalty of 0.5 dB for the ideal receiver and 0.7 dB for the proposed algorithm. The penalty difference of 0.2 dB is thus the implementation-induced penalty. For 16-QAM the minimum penalties decreases (0.4 dB for the ideal receiver, 0.6 dB for the proposed algorithm), because only 2 out of 4 transmitted bits are differentially encoded. For all 4 receivers it can be seen that almost no additional penalty is induced due to the quantization of the carrier phase, provided that $\log_2\{B\} \geq 5$. Therefore, in all following simulations for 4-QAM and 16-QAM B is set to 32.

Fig. 6(b) shows the same simulations for 64-QAM and 256-QAM. The minimum penalty for 64-QAM is 0.3 dB with ideal carrier recovery and 0.5 dB using the proposed algorithm. For 256-QAM the respective values are 0.35 dB and 0.55 dB. For both constellations the penalty due to the quantization of the carrier phase is tolerable only if $\log_2\{B\} \geq 6$. The number of test phase values for 64-QAM and 256-QAM is therefore chosen to be $B = 64$ in all subsequent simulations.

B. Phase Noise Tolerance

Another important property of a carrier recovery in a coherent receiver is its tolerance against phase noise. Today's commercial transmission systems usually employ DFB lasers, because they are cost-efficient and have a small footprint. The linewidth of such lasers is in the range of 100 kHz $< \Delta f_{\mathrm{DFB}} <$ 10 MHz. Assuming a symbol rate of 10 Gbaud the tolerable sum linewidth times symbol duration product must be $10^{-5} < 2\Delta f_{\mathrm{DFB}} \cdot T_S < 10^{-3}$.

Fig. 7 shows the sensitivity penalty of the proposed carrier recovery algorithm against the linewidth times symbol duration product. Table I lists the maximum tolerable linewidth times symbol duration product for a sensitivity penalty of 1 dB at a BER of 10^{-3}. In a polarization multiplexed system with the same common carrier recovery for both polarizations (as described in Section III.C), these values can be approximately doubled.

In order to evaluate the phase noise tolerance of the algorithm also for lower BER rates, additional long term simulations have been executed for selected values of $\Delta f \cdot T_S$, simulating 2 000 000 symbols per data point (Fig. 8). Note that for BERs below 10^{-5} the results become inaccurate due to the low number of errors that occurred during simulation. The theoretical optimum is calculated by inverting (17), which results in the following equation:

$$\mathrm{BER} = 1 - \left(1 - \frac{2}{\log_2\{M\}}\left(1 - \frac{1}{\sqrt{M}}\right)\mathrm{Q}\left[\sqrt{\frac{3}{M-1}\frac{E_S}{N_0}}\right]\right)^2 \tag{18}$$

It can be seen that for the values of $\Delta f \cdot T_S$ causing 1 dB of penalty at a BER of 10^{-3}, the penalty increases for lower BERs, especially for higher order QAM constellations. But if these values are reduced to one quarter the penalty stays almost constant even for BER rates down to 10^{-5}.

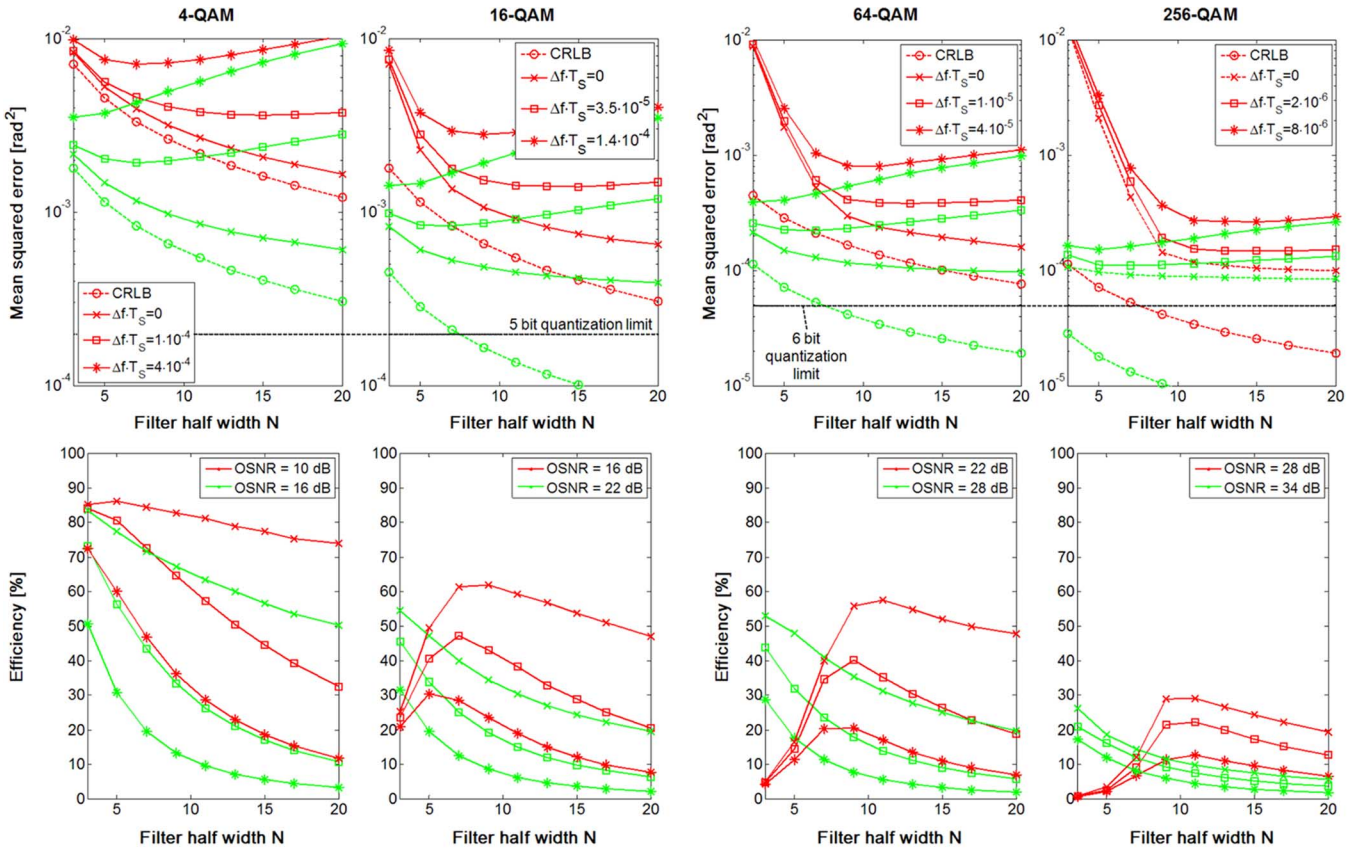

Fig. 9. Phase estimator mean squared error and efficiency $e(N)$ versus filter half width N for different square QAM constellations. (The legends apply to both figures of a column.).

C. Carrier Phase Estimator Efficiency

In the following the efficiency of the phase estimator is analyzed. For high OSNR the contribution of AWGN to phase noise can be considered to be also Gaussian with the variance $(2E_S/N_0)^{-1}$ [23]. Therefore, the efficiency $e(N)$ of the phase estimator depending on the filter half width N is given by

$$e(N) = \frac{\frac{1}{2N+1}\left(2\frac{E_S}{N_0}\right)^{-1}}{\langle(\psi - \hat{\psi})^2\rangle} \leq 1 \tag{19}$$

where the numerator is the Cramér–Rao lower bound (CRLB) [24], and the denominator is the mean squared error of the phase estimator output. The CRLB is independent of the estimator structure and specifies the lowest possible mean squared error achievable by an unbiased estimator. Thus, the maximum estimator efficiency is 1.

Fig. 9 shows the mean squared error together with the theoretical optimum expressed by the CRLB (top row) and the resulting estimator efficiency $e(N)$ (bottom row) for the proposed carrier recovery concept and different square QAM constellations.

For all considered constellations in the absence of phase noise the mean squared error $\langle(\psi - \hat{\psi})^2\rangle$ continuously decreases for larger values of N. In contrast if phase noise is present a global minimum emerges that depends on the linewidth times symbol duration products the OSNR. It can be seen that $N = 9$, which was selected for our simulations, induces a mean squared error that is always close to this minimum, especially for lower OSNRs. In principle by optimizing N for each parameter set $\{\text{OSNR}, \Delta f \cdot T_S, M\}$ the performance of the receiver could have been improved. But as this is not practical in real systems this optimization was omitted in the simulations.

A result comparison among the different QAM constellations makes it apparent that the maximum achievable efficiency reduces from $\sim$ 85% for 4-QAM to $\sim$ 60% for 16-QAM and 64-QAM to finally around 30% for 256-QAM. This reduction is mainly caused by the quantization of the carrier phase that limits the minimum achievable mean squared error of the estimator. For $\log_2\{B\} = 5$ (4-QAM, 16-QAM) and $\log_2\{B\} = 6$ (64-QAM, 256-QAM) the minimum mean squared errors are $2 \cdot 10^{-4}$ rad^2 and $5 \cdot 10^{-5}$ rad^2, respectively. For 4-QAM the CRLB is well above the quantization limit, thus quantization effects can mostly be neglected. For 16-QAM and 64-QAM the CRLB is in the range of the quantization limit. Hence, the estimator efficiency is already reduced, especially for low OSNR. If the resolution of the carrier phase for 16-QAM is increased to 6 bit, the estimator efficiency improves to $\sim$80%. Finally for 256-QAM the CRLB is mostly below the 6 bit quantization limit, which of course severely degrades the estimator efficiency. Increasing the carrier phase resolution would cause an improvement. But as can be seen from Fig. 8 the achieved mean squared errors are already sufficient to reliably recover 256-QAM symbols.

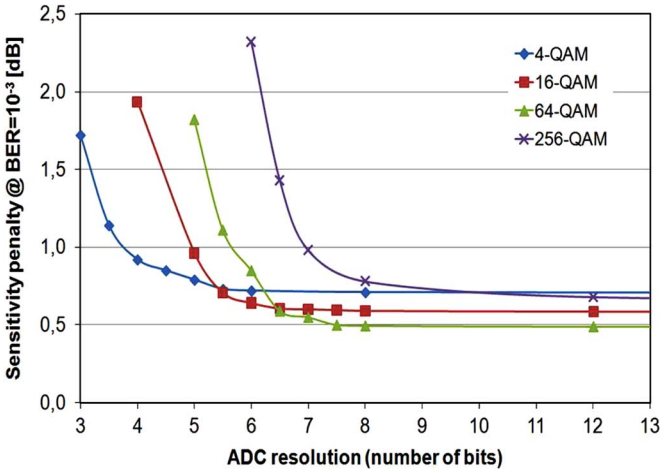

Fig. 10. Receiver sensitivity penalty versus analog-to-digital converter resolution for different square QAM constellations.

Another peculiarity is that the efficiency for higher order QAM constellations tends to go to zero for short filter lengths and low OSNR. The reason for this effect becomes obvious if one recalls the carrier recovery algorithm: The squared distance of the received symbol to the closest constellation point is calculated for different carrier phase angles. Looking at the developing of $|d_{k,b}|^2$ over the different φ_b the algorithm produces for 4-QAM one distinct minimum even for $N = 0$. In contrast for higher order QAM constellations several local minima will emerge. Therefore, larger filters are required to identify the global minimum, especially for lower OSNRs where the signal is stronger corrupted by noise.

D. Analog-To-Digital Converter Resolution

Next to phase noise tolerance another major obstacle to realize realtime coherent transmission systems with digital carrier recovery is based on the required bandwidth and resolution of the analog-to-digital converter (ADC). Fig. 10 shows the effect of the ADC resolution on the receiver sensitivity for the considered QAM constellations. The necessary ADC resolution increases approximately by 1 bit if the number of constellation points is multiplied by 4. This relation becomes evident by looking again at Fig. 1. It can be seen that increasing the number of constellations points by a factor of 4 doubles the size of the constellation diagram in Re- and Im-dimensions. Therefore, to keep the accuracy of the received samples constant, the number of ADC quantization steps must also double. Table II summarizes the ADC requirements for a 100 Gb/s polarization multiplexed transmission system. Since commercial systems will also contain PMD and CD compensation, which necessitates oversampling, the values for $T_S/2$ sampling are also given.

E. Internal Resolutions

Not only the external quantization limited by the ADC resolution constrains algorithm performance, but also internal resolutions have to be considered. Therefore, an optimal compromise must be found between performance degradation and hardware efficiency. Especially because the proposed algorithm uses

TABLE II
ANALOG-TO-DIGITAL CONVERTER REQUIREMENTS FOR POLARIZATION MULTIPLEXED 100 GB/S TRANSMISSION

Constellation	ADC bandwidth	ADC sampling rate ($T_S/2$ sampling)	ADC effective number of bits
4-QAM	25 GHz	50 Gsamples/s	> 3.8
16-QAM	12.5 GHz	25 Gsamples/s	> 4.9
64-QAM	8.33 GHz	16.67 Gsamples/s	> 5.7
256-QAM	6.25 GHz	12.5 Gsamples/s	> 7.0

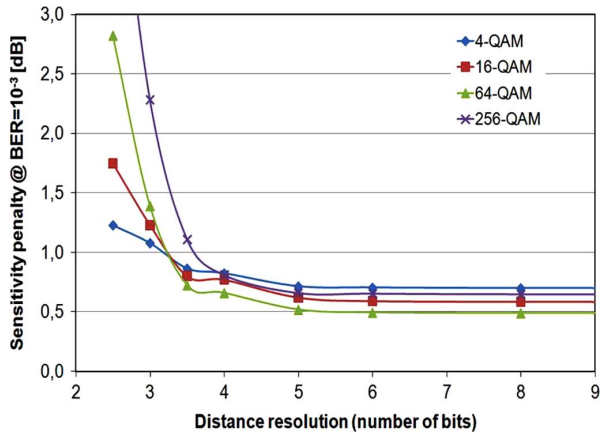

Fig. 11. Receiver sensitivity penalty versus internal resolution for the distances $\mathrm{Re}[d_{k,b}]$ and $\mathrm{Im}[d_{k,b}]$ for different square QAM constellations.

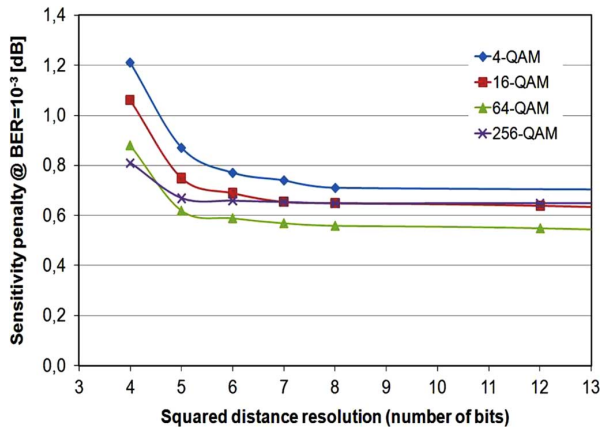

Fig. 12. Receiver sensitivity penalty versus internal resolution for the squared distance $|d_{k,b}|^2$ for different square QAM constellations.

B parallel blocks per module, the hardware efficiency of each block is crucial for the practicality of the system.

To find an efficient hardware implementation, one important goal is to avoid multipliers in the system, since they usually utilize a lot of chip area. Fig. 11 shows the receiver sensitivity penalty against different resolutions of $\mathrm{Re}[d_{k,b}]$ and $\mathrm{Im}[d_{k,b}]$. The results are similar for all considered constellations and show, that a resolution $\geq$ 4 bits is sufficient. As for $|d_{k,b}|^2$ the penalty for a resolution ≥ 5 bits is tolerable (Fig. 12), the $(\,)^2$-operation in (16) can be realized with a small look-up table (4 bit input, 4 bit output) or simple logic functions.

The reason for the similar results for all simulated constellations is that the distance to the closest constellation point is independent of the number of constellation points. This fact was

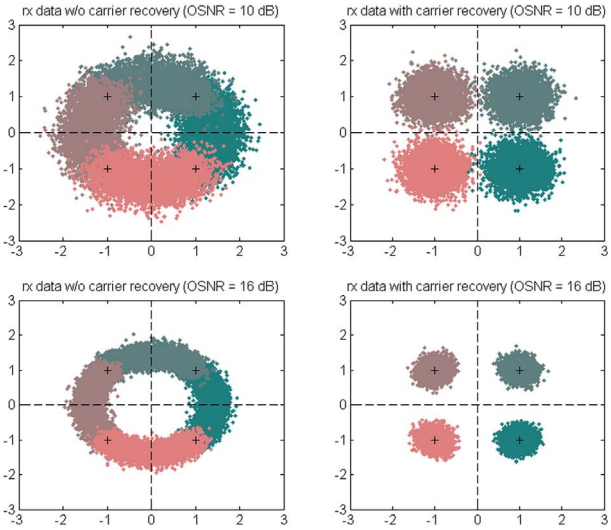

Fig. 13. 4-QAM constellation diagram at the receiver before and after carrier recovery for $\Delta f \cdot T_S = 4.1 \cdot 10^{-4}$.

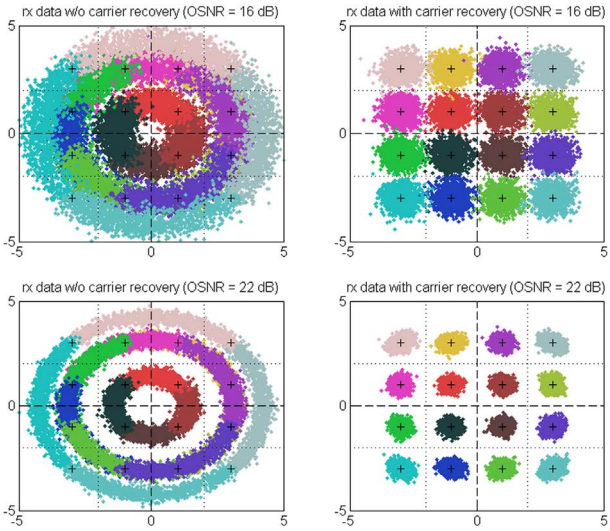

Fig. 14. 16-QAM constellation diagram at the receiver before and after carrier recovery for $\Delta f \cdot T_S = 1.4 \cdot 10^{-4}$.

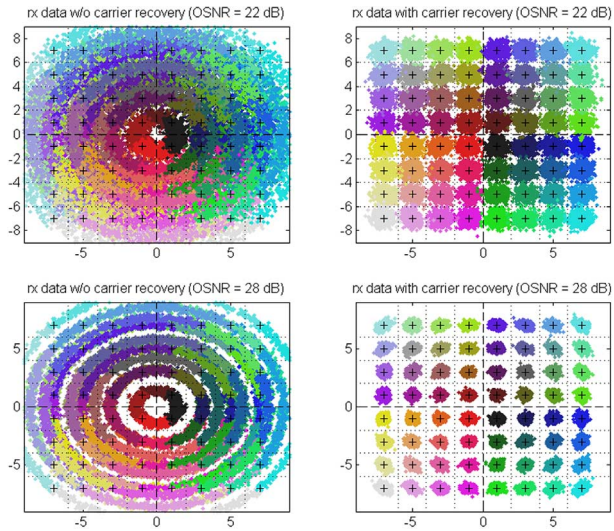

Fig. 15. 64-QAM constellation diagram at the receiver before and after carrier recovery for $\Delta f \cdot T_S = 4.0 \cdot 10^{-5}$.

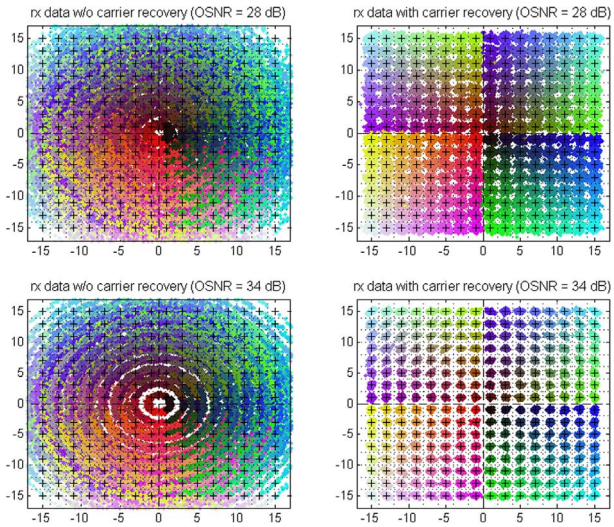

Fig. 16. 256-QAM constellation diagram at the receiver before and after carrier recovery for $\Delta f \cdot T_S = 8.0 \cdot 10^{-6}$.

already mentioned in Section IV.B and shows that the hardware effort to implement the proposed algorithm only increases moderately for higher order QAM constellations. The needed internal resolutions for calculation of $|d_{k,b}|^2$ and consequently also for the subsequent filter function is always the same. Therefore, the proposed feedforward carrier recovery algorithm becomes hardware-efficient especially for high order QAM constellations.

VI. Discussion

To demonstrate the feasibility of optical high-order QAM transmission Figs. 13–16 depict the constellation diagrams at the receiver before and after carrier recovery for the investigated square QAM formats. The OSNRs are the same as in Section V.C. The figures show that the carrier phase can be reliably recovered by the proposed feedforward algorithm, even for high order QAM constellations.

A potential implementation of such transmission systems with cost-effective DFB lasers will make them very attractive for future commercialization. Furthermore, the growth of transmission bandwidth in existing optical fiber systems will only be viable by increasing the spectral efficiency using advanced modulation formats. Therefore, QAM will play an important role for systems supporting 100 Gb/s, 400 Gb/s, or even higher data rates.

There are two main technological barriers remaining to successfully develop a high-order QAM transceiver. The first one is the availability of low-cost low linewidth DFB lasers. But the results in Table I show that the requirements for the laser linewidth are not as stringent as one would expect. DFB lasers with a linewidth of 10 kHz are available today [25], consequently allowing even an implementation of 256-QAM.

The second technological barrier is the requisite ADC bandwidth and resolution. Table II showed corresponding values required for the realization of a coherent polarization-multiplexed 100 Gb/s system. State-of-the-art ADCs already accomplish sampling rates above 10 GS/s [26]–[28], enabling

realtime 10 Gbaud 4-QAM (QPSK) systems [29]. But the effective resolution is limited to $\sim$ 5 bits and ADCs with the required higher resolutions are limited to lower sampling rates [30], [31], therefore inhibiting the implementation of 64-QAM or even 256-QAM. However, further developments in ADC design [32] and device technology will enable the realization of these high-order QAM modulation formats in optical transmission systems in the near future.

VII. Summary

In this paper a novel phase noise tolerant feedforward carrier recovery concept for arbitrary M-QAM constellations was presented and a hardware-efficient implementation of the algorithm was proposed. A tolerance against linewidth times symbol rate products of $4.1 \cdot 10^{-4}$, $1.4 \cdot 10^{-4}$, $4.0 \cdot 10^{-5}$, and $8.0 \cdot 10^{-6}$ for a penalty of 1 dB at a BER of 10^{-3} for square 4-QAM, 16-QAM, 64-QAM and 256-QAM, respectively, was determined by Monte Carlo simulation.

References

[1] E. Ip, A. Lau, D. Barros, and J. Kahn, "Coherent detection in optical fiber systems," *Opt. Exp.*, vol. 16, no. 2, pp. 753–791, Jan. 09, 2008.

[2] G. Charlet, J. Renaudier, H. Mardoyan, P. Tran, O. Pardo, F. Verluise, M. Achouche, A. Boutin, F. Blache, J. Dupuy, and S. Bigo, "Transmission of 16.4 Tbit/s capacity over 2 550 km using PDM QPSK modulation format and coherent receiver," in *Proc. OFC/NFOEC'08*, San Diego, CA, Feb. 24–28, 2008, PDP3.

[3] T. Pfau, R. Peveling, J. Hauden, N. Grossard, H. Porte, Y. Achiam, S. Hoffmann, S. Ibrahim, O. Adamczyk, S. Bhandare, D. Sandel, M. Porrmann, and R. Noé, "Coherent digital polarization diversity receiver for real-time polarization-multiplexed QPSK transmission at 2.8 Gbit/s," *IEEE Photon. Technol. Lett.*, vol. 19, no. 24, pp. 1988–1990, Dec. 15, 2007.

[4] A. Leven, N. Kaneda, and Y. Chen, "Real-time CMA-based 10 Gb/s polarization demultiplexing coherent receiver implemented in an FPGA," in *Proc. OFC/NFOEC'08*, San Diego, CA, USA, Feb. 24–28, 2008, OTuO2.

[5] L. Nelson, S. Woodward, M. Feuer, X. Zhou, P. Magill, S. Foo, D. Hanson, D. McGhan, H. Sun, M. Moyer, and M. O'Sullivan, "Performance of a 46-Gbps dual-polarization QPSK transceiver in a high-PMD fiber transmission experiment," in *Proc. OFC/NFOEC'08*, San Diego, CA, Feb. 24–28, 2008, PDP9.

[6] T. Sakamoto, A. Chiba, and T. Kawanishi, "50-Gb/s 16 QAM by a quad-parallel mach-zehnder modulator," in *Proc. ECOC'07*, Berlin, Germany, Sep. 16–20, 2007, PD 2.8.

[7] C. Doerr, P. Winzer, L. Zhang, L. Buhl, and N. Sauer, "Monolithic InP 16-QAM modulator," in *Proc. OFC/NFOEC'08*, San Diego, CA, Feb. 24–28, 2008, PDP20.

[8] H. Goto, K. Kasai, M. Yoshida, and M. Nakazawa, "Polarization-multiplexed 1 Gsymbol/s, 128 QAM (14 Gbit/s) coherent optical transmission over 160 km using a 1.4 GHz nyquist filter," in *Proc. OFC/NFOEC'08* , San Diego, CA, Feb. 24–28, 2008, JThA45.

[9] A. Tarighat, R. Hsu, A. Sayed, and B. Jalali, "Digital adaptive phase noise reduction in coherent optical links," *J. Lightw. Technol.*, vol. 24, no. 3, pp. 1269–1276, Mar. 2006.

[10] E. Ip and J. Kahn, "Feedforward carrier recovery for coherent optical communication," *J. Lightw. Technol.*, vol. 25, no. 16, pp. 2675–2692, Sep. 2007.

[11] H. Louchet, K. Kuzmin, and A. Richter, "Improved DSP algorithms for coherent 16-QAM transmission," in *Proc. ECOC'08*, Brussels, Belgium, Sep. 21–25, 2008, Tu.1.E.6.

[12] M. Seimetz, "Laser linewidth limitations for optical systems with high-order modulation employing feed forward digital carrier phase estimation," in *Proc. OFC/NFOEC'08*, San Diego, CA, Feb. 24–28, 2008, OTuM2.

[13] U.-V. Koc, "PLL-free quadrature-amplitude modulation in coherent optical communication," in *Proc. ISCAS'07*, New Orleans, LA, May 27–30, 2007, pp. 2299–2302.

[14] F. Munier, E. Alpman, T. Eriksson, A. Svensson, and H. Zirath, "Estimation of phase noise for QPSK modulation over AWGN channels," in *Proc. GigaHertz 2003 Symp.*, Linköping, Sweden, Nov. 4–5, 2003.

[15] E. Cacciamani and C. Wolejsza, "Phase-ambiguity resolution in a four-phase PSK communications system," *IEEE Trans. Commun. Techn.*, vol. 19, no. 6, pp. 1200–1210, Dec. 1971.

[16] W. Weber, "Differential encoding for multiple amplitude and phase shift keying systems," *IEEE Trans. Commun.*, vol. 26, no. 3, pp. 385–391, Mar. 1978.

[17] R. Noé, "PLL-free synchronous QPSK polarization multiplex/diversity receiver concept with digital I&Q baseband processing," *IEEE Photon. Technol. Lett.*, vol. 17, no. 4, pp. 887–889, Apr. 2005.

[18] W. Webb and L. Hanzo, *Modern Quadrature Amplitude Modulation*. London, U.K.: Pentech Press, 1994.

[19] R. Noé, "Phase noise tolerant synchronous QPSK/BPSK baseband-type intradyne receiver concept with feedforward carrier recovery," *J. Lightw. Technol.*, vol. 23, no. 2, pp. 802–808, Feb. 2005.

[20] K. Kikuchi, "Polarization-demultiplexing algorithm in the digital coherent receiver," in *Proc. SUM'08*, Acapulco, Mexico, Jul. 21–23, 2008, MC2.2.

[21] J. Volder, "The CORDIC trigonometric computing technique," *IRE Trans. on Electron. Comp.*, vol. EC-8, no. 3, pp. 330–334, 1959.

[22] J. Walther, "A unified algorithm for elementary functions," in *Proc. Spring Joint Comp. Conf.*, Atlantic City, NJ, May 18–20, 1971, pp. 379–385.

[23] S. Tretter, "Estimating the frequency of a noisy sinusoid by linear regression," *IEEE Trans. Inf. Theory*, vol. 31, no. 6, pp. 832–835, Nov. 1985.

[24] H. Cramér, *Mathematical Methods of Statistics*. : Princeton University Press, Mar. 23, 1999.

[25] *Sabeus Precision Advantage™ AG-1 Source Laser Datasheet*. Calabasas, CA: Sabeus Inc., 2006.

[26] K. Poulton, R. Neff, B. Setterberg, B. Wuppermann, T. Kopley, R. Jewett, J. Pernillo, C. Tan, and A. Montijo, "A 20 GS/s 8b ADC with a 1 MB memory in 0.18 μm CMOS," in *Proc. ISSCC'03*, San Francisco, CA, Feb. 9–13, 2003, 18.1.

[27] H. Nosaka, M. Nakamura, K. Sano, M. Ida, K. Kurishima, T. Shibata, M. Tokumitsu, and M. Muraguchi, "A 24-Gsps 3-bit nyquist ADC using InP HBTs for DSP-based electronic dispersion compensation," *IEICE Trans. Electron.*, vol. E88-C, no. 6, pp. 1125–1232, Jun. 2005.

[28] O. Adamczyk and R. Noé, "13 Gsamples/s 5-bit analogue-to-digital converter for coherent optical QPSK receiver," *Electron. Lett.*, vol. 44, pp. 895–896, 2008.

[29] H. Sun, K. Wu, and K. Roberts, "Real-time measurements of a 40 Gb/s coherent system," *Opt. Exp.*, vol. 16, no. 2, pp. 873–879, Jan. 2008.

[30] F. Boré, S. Bruel, and M. Wingender, "A 10-bit 2.2 Gsps ADC operating over first and second nyquist zones," *Atmel Appl.*, no. 6, pp. 43–48, Winter 2006.

[31] B. Chan, B. Oyama, C. Monier, and A. Gutierrez, "An ultra-wideband 7-bit 5 Gsps ADC implemented in submicron InP HBT technology," in *Proc. CSIC'07*, Portland, OR, Oct. 14–17, 2007, O.4.

[32] T. Ellermeyer, J. Mullrich, J. Rupeter, H. Langenhagen, and A. Bielik, "DA and AD converters for 25 GS/s and above," in *Proc. SUM'08*, Acapulco, Mexico, Jul. 21–23, 2008, TuC3.1.

Timo Pfau (S'08) was born in Stuttgart, Germany, in 1979. He received the Dipl.-Ing. degree in electrical engineering and information technology from the University of Stuttgart, Germany, in 2004. After graduation he was granted a scholarship from the International Graduate School "Dynamic Intelligent Systems" of the University of Paderborn, Germany, where he joined the working group "Optical Communication and High Frequency Engineering" of Prof. Noé. There he is currently working towards the Dr.-Ing. degree focusing on the development and implementation of realtime coherent lightwave systems with DFB lasers.

Mr. Pfau is a member of the VDE Association for Electrical, Electronic & Information Technologies and serves as a reviewer for IEEE Photonics Technology Letters and IEEE Journal of Lightwave Technology.

Sebastian Hoffmann was born in Bielefeld, Germany, in 1969. He received the Dipl.-Ing., Dipl.-Wirt.-Ing., and Dr.-Ing. degrees from the University of Paderborn, Paderborn, Germany, in 1997, 2000, and 2008, respectively.

After vocational training as a power electronics technician from 1988 to 1991 at Miele & Cie. KG, Bielefeld, Germany, he studied electrical engineering in Paderborn, Germany and Waterloo, Canada. After graduation he stayed in the research group of Prof. Noé as a postdoctoral researcher. He has contributed to various projects including microelectronics, high frequency engineering and optical communication.

Reinhold Noé (M'93) was born in Darmstadt, Germany, in 1960. He received the Dipl.-Ing. and Dr.-Ing. degrees in electrical engineering from Technische Universität München (Munich), Germany, in 1984 and 1987, respectively.

At that time, he realized the first endless polarization control systems. Then he spent a postdoctoral year with Bellcore, Red Bank, NJ, where he continued to work on coherent optical systems. In 1988 he joined Siemens Research Laboratories, Munich. In 1992, he implemented the first synchronous optical PSK transmission with normal DFB lasers. Since 1992, he is the Chair of Optical Communication and High-Frequency Engineering, University of Paderborn, Germany. Most of his recent experiments deal with PMD/CD detection and compensation, optical polarization control and realtime synchronous QPSK transmission.